electronics

MDPI

Article

Towards a Digital Twin of Coronary Stenting: A Suitable and Validated Image-Based Approach for Mimicking Patient-Specific Coronary Arteries

Gianluca Poletti [1], Luca Antonini [1], Lorenzo Mandelli [1], Panagiota Tsompou [2], Georgia S. Karanasiou [2,3], Michail I. Papafaklis [4], Lampros K. Michalis [5], Dimitrios I. Fotiadis [2,3], Lorenza Petrini [6,*] and Giancarlo Pennati [1]

[1] Department of Chemistry, Materials and Chemical Engineering "Giulio Natta", Politecnico di Milano, Piazza Leonardo da Vinci 32, 20133 Milano, Italy; gianluca.poletti@polimi.it (G.P.); luca.antonini@polimi.it (L.A.); lorenzo.mandelli@polimi.it (L.M.); giancarlo.pennati@polimi.it (G.P.)
[2] Department of Materials Science and Engineering, University of Ioannina, 45110 Ioannina, Greece; panagiotatsompou@gmail.com (P.T.); g.karanasiou@gmail.com (G.S.K.); fotiadis@cs.uoi.gr (D.I.F.)
[3] Department of Biomedical Research Institute—FORTH, University Campus of Ioannina, 45110 Ioannina, Greece
[4] 2nd Department of Cardiology, University Hospital of Ioannina, 45110 Ioannina, Greece; m.papafaklis@yahoo.com
[5] Faculty of Medicine, School of Health Sciences, University of Ioannina, 45110 Ioannina, Greece; lamprosmihalis@gmail.com
[6] Department of Civil and Environmental Engineering, Politecnico di Milano, Piazza Leonardo da Vinci 32, 20133 Milano, Italy
* Correspondence: lorenza.petrini@polimi.it

Citation: Poletti, G.; Antonini, L.; Mandelli, L.; Tsompou, P.; Karanasiou, G.S.; Papafaklis, M.I.; Michalis, L.K.; Fotiadis, D.I.; Petrini, L.; Pennati, G. Towards a Digital Twin of Coronary Stenting: A Suitable and Validated Image-Based Approach for Mimicking Patient-Specific Coronary Arteries. *Electronics* **2022**, *11*, 502. https://doi.org/10.3390/electronics11030502

Academic Editor: Abdeldjalil Ouahabi

Received: 18 December 2021
Accepted: 3 February 2022
Published: 8 February 2022

Abstract: Considering the field of application involving stent deployment simulations, the exploitation of a digital twin of coronary stenting that can reliably mimic the patient-specific clinical reality could lead to improvements in individual treatments. A starting step to pursue this goal is the development of simple, but at the same time, robust and effective computational methods to obtain a good compromise between the accuracy of the description of physical phenomena and computational costs. Specifically, this work proposes an approach for the development of a patient-specific artery model to be used in stenting simulations. The finite element model was generated through a 3D reconstruction based on the clinical imaging (coronary Optical Coherence Tomography (OCT) and angiography) acquired on the pre-treatment patient. From a mechanical point of view, the coronary wall was described with a suitable phenomenological model, which is consistent with more complex constitutive approaches and accounts for the in vivo pressurization and axial pre-stretch. The effectiveness of this artery modeling method was tested by reproducing in silico the stenting procedures of two clinical cases and comparing the computational results with the in vivo lumen area of the stented vessel.

Keywords: coronary stent; stent deployment simulation; finite element analysis; patient-specific cases; validation; artery model; 3D reconstruction; plaque characterization

1. Introduction

Coronary artery disease is the leading cause of death among cardiovascular pathologies, with stenting being the most common treatment [1]. The treatment consists of a minimally invasive surgical procedure, which, through balloon dilation and stent implantation, aims to restore the physiological lumen in coronary arteries narrowed by atherosclerotic plaque. Several stent types and clinical procedures were evaluated in the last decades, leading to the current gold standard of drug-eluting stent implantation. Nevertheless, there still remain risks of treatment failure due to in-stent restenosis and stent

thrombosis. The occurrence of these adverse events is mainly correlated to the presence of arterial injury during treatment and stent malapposition at the end of the surgical procedure [2]. Both phenomena are related to the mechanical interaction between the device and the patient-specific arteries in the acute phase of treatment.

Finite element analysis (FEA) of the stent deployment is a useful tool that can be used for investigating the potential causes of these adverse events. Several literature works showed that through numerical simulations, different types of evaluation could be performed, including the prediction of treatment outcomes, the assessment of device performances, or the optimization of clinical procedures [3–8], using either generic anatomies or patient-specific features. Having a virtual representation of the patient-specific case that allows for these kinds of evaluations would be a great step forward in improving individual treatments [3,9,10].

This approach evokes the so-called "digital twin", which is nowadays well established in industry where it is used to indicate a virtual representation of a physical product, such as an engine or an aerospace vehicle. A digital twin is developed to monitor real-time the product and obtain virtual insights and data for the optimization of design or control processes [11]. The concept of the digital twin was recently introduced in the biomedical context and, with particular interest for the current work, in interventional cardiology, where the development of a digital twin can improve clinical decisions, specifically supporting disease diagnosis, guiding treatments, or evaluating prognosis [12]. Some virtual representations of patient-specific cases have already reached clinical adoption. A remarkable example is the HeartFlow FFR$_{CT}$ Analysis (HeartFlow, Redwood City, CA, USA), which through clinical measurements generates patient-specific 3D models of blood flow across the diseased coronary arterial tree to calculate clinically relevant diagnostic indexes (the fractional flow reserve) [13]. However, virtual representations involving clinical data seem partially inconsistent with typical features of the industrial-use digital twin: indeed, continuous data acquisition and real-time interaction between physical objects and virtual models cannot be achieved in most cases.

Another crucial aspect to consider when developing a virtual representation is the reliability of numerical results, which must be guaranteed by the employment of an appropriate validation strategy of the numerical models. Most of the literature studies concerning the modeling of stent deployment in coronary arteries focused on the development of virtual scenarios to compare the performance of different devices or clinical procedures, often not adequately supported by the validation of the models employed. Validating a stent deployment model that involves a patient-specific case implies acquiring patient data, simulating the treatment, and then comparing the in silico outputs with the clinical observations. Only a very limited number of scientific works replicated a clinical case of coronary stent deployment, exploiting information available from in vivo images, and tried to compare, at least qualitatively, the simulation outcomes with data from real clinical studies [3,7].

When approaching the simulation of patient-specific coronary stenting, one of the main difficulties is in the modeling of the artery, which unlike devices and clinical procedures to be replicated, is always affected by unavoidable uncertainties. Indeed, although the in vivo image processing allows the 3D reconstruction of the arterial patient-specific anatomy and plaque components distribution, average mechanical behaviors from literature data have to be assumed for the various vessel components as their measure in vivo on the patient is impossible. Different models were proposed in the literature for the arterial mechanical behavior, ranging from complex constitutive models [14], suitable for idealized geometries, to simpler phenomenological models, more easily applicable to patient-specific geometries [3,7,8]. A further aspect is to be considered when modeling the mechanical behavior of in vivo coronary artery, namely the vessel pre-stretching and pressurization under physiological conditions. Although the geometry derived from clinical images is representative of an in vivo stressed configuration, this is generally not accounted for in the arterial modeling, and the constitutive parameters of material models

are based on experimental tests performed on unloaded layers of coronary tissue [3–5,7,8,15,16].

For these reasons, this paper focuses on the definition of a smart methodological approach for modeling patient-specific coronary arteries to be used for a virtual representation of coronary stenting. Furthermore, the study aims to evaluate the model reliability by quantitative comparison with clinical data collected immediately after the stenting treatment. Specifically, the arterial models were developed based on patient-specific clinical images. Their mechanical behavior was described adopting a phenomenological model, capable through a simple and effective method of accounting for the plaque heterogeneity and in vivo condition of the coronary artery. The availability of two clinical cases with detailed information on the procedure and in vivo images pre- and post-stent deployment allowed a faithful replication of the treatment and quantitative comparison between model results and clinical data. The final goal of this work is to allow the use of virtual representation of coronary stenting as a tool for aiding clinical decisions, supported by a new conceptualization of the digital twin in the biomedical field.

2. Materials and Methods

2.1. Finite Element Model of Patient-Specific Coronary Arteries

2.1.1. From the Clinical Images to the 3D Reconstruction

An ad hoc methodology was implemented for the accurate reconstruction of the artery and plaques from OCT (St. Jude Medical, Inc., Saint Paul, MN, USA) images. For the lumen detection, the following process was applied: (i) pre-processing; (ii) guidewire removal; (iii) bilateral filtering application to smooth out any residual noise and enhance the lumen border; and (iv) application of a fast marching algorithm, for the lumen extraction. For the segmentation of the outer border, the methodology was based on the detection of the sharp transition effect between bright areas representing the tissue to dark areas representing background pixels. The first step was the bilateral filtering of the OCT frame. Next, standard deviation filtering of each image on a 11 × 11 neighborhood was performed. The final step of the methodology was to apply Frangi's vesselness filter [17] on the image of the standard deviation. It allowed finding the outer border corresponding to the external elastic lamina (EEL), the tissue that divides the media and the adventitia.

For the characterization of the different plaque types, a new methodology was developed, that is based on deep learning techniques and specifically convolutional neural networks (CNN). More specifically, a convolutional neural network was trained to identify 4 different types of plaques from OCT images (calcified plaque (CA), fibrous tissue (FT), lipid tissue (LT), mixed tissue (MT)), as can be seen in Figure 1b. The plaque characterization step was executed right after the extraction of the lumen and borders because the methodology needs the definition of the region of interest (ROI) of the tissue where the neural network is applied and trained. For the sake of completeness, it should be pointed out that the CNN generates predictions for five classes: four classes representing the four plaque types (CA, FT, LT, MT) and one class (background (BK)) representing the rest of the pixels, e.g., catheter shadow pixels, healthy tissue pixels. The process includes the following steps: (i) determination of the ROI; (ii) patch cropping of the ROI; (iii) feeding the patches to the CNN; (iv) CNN outputs the inference in the form of probability scores for each class.

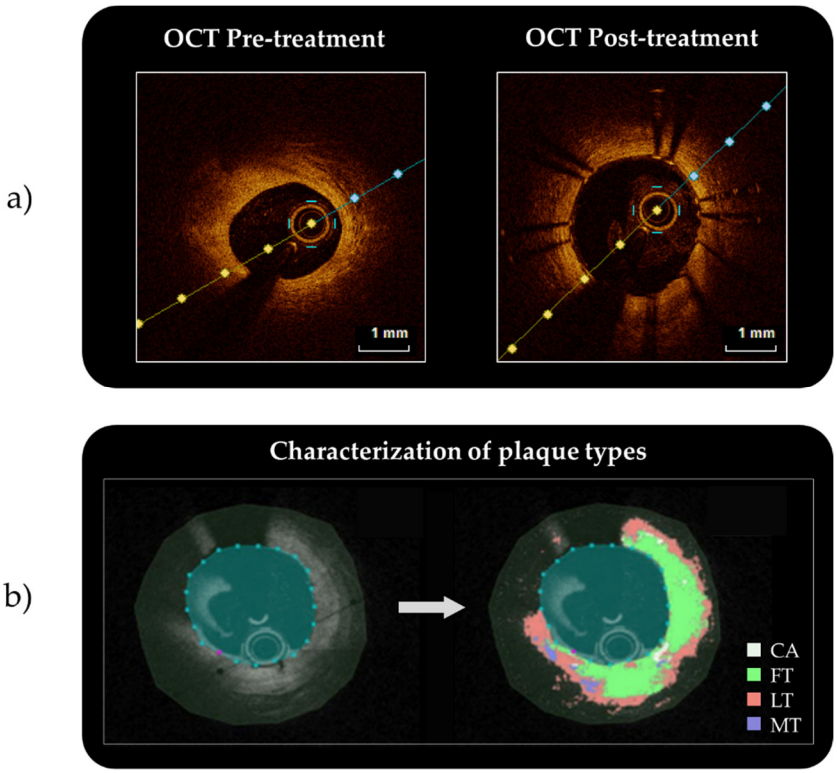

Figure 1. OCT images were used for the reconstruction of the patient-specific artery and plaque: (**a**) good OCT image quality was required both for the reconstruction of the artery from the OCT pre-treatment images and for the quantitative comparison of the OCT post-treatment lumen areas and model results; (**b**) a CNN was used to characterize the plaque types (calcified plaque (CA), fibrous tissue (FT), lipid tissue (LT), mixed tissue (MT)) from patient OCT images.

Following the segmentation of the inner and outer borders and plaques, the extraction of the 2D centerline and borders of the targeted portion of the artery on two angiographic projections (X-ray Biplane Angiographies, Philips Allura Xper) was performed [18]. Next, the 2D dimensional data from both views were combined to obtain the 3D centerline path. By combining the 3D centerline path information (i.e., vessel curvature and torsion) obtained from X-ray Angiography with the cross-sectional data obtained from OCT, geometrically correct 3D models of the artery and plaques were obtained. The process can be summarized as follows: (i) extraction of the 3D centerline path from biplane angiographies; (ii) segmentation of OCT frames to obtain 2D locations of lumen/wall/plaques; (iii) mapping of the 2D frames on the catheter path; (iv) calculation of the relative catheter twist; (v) calculation of the absolute frame orientation; and (vi) visualization or quantification of the 3D models.

2.1.2. Discretization of the 3D Reconstructed Geometries

The reconstruction method generated two 3D surfaces in .stl format: the inner surface (i.e., the surface representing the artery lumen) and an external surface (corresponding to the external elastic lamina (EEL)). The EEL surface was taken as a reference for the identification of the artery tissue layers, namely the diseased intima, the media, and the adventitia. The thickness of media and adventitia was related to the EEL mean diameter with two coefficients, $\alpha = 0.0890$ and $\mu = 0.0838$, whose values were identified based on the literature work by Holzapfel et al. (2005) [19]:

$$t_{ADVENTITIA} = \alpha \cdot D_{EEL} \quad (1)$$

$$t_{MEDIA} = \mu \cdot D_{EEL} \quad (2)$$

where $t_{ADVENTITIA}$ and t_{MEDIA} stands for the thickness of the two artery layers and D_{EEL} corresponds to the EEL mean diameter. The surfaces representing the internal elastic lamina (IEL), i.e., the interface between the intima and the media, and the outer surface of the adventitia were obtained as offsets of the EEL surface: an internal offset with thickness value equal to t_{MEDIA} was used to generate the IEL, while the outer surface was obtained with an external offset with a thickness value equal to $t_{ADVENTITIA}$. In this way, it was possible to identify the three volumes representing the artery layers: the adventitia between the outer surface and the EEL, the media between the EEL and the IEL, and the diseased intima between the IEL and the lumen surface. Each layer was meshed with hexahedral elements through ANSA Pre Processor v20.0 (BETA CAE Systems, Root, Switzerland) and, to have an almost homogeneous dimension of the elements, two elements were considered in the thickness of both the adventitia and the media, and four elements for the diseased intima.

In addition to the identification of the lumen and the EEL surfaces by the 3D reconstruction method, it was also possible to detect the presence of four different plaque components and each of them was associated to point clouds in which each point was described by its three spatial coordinates. Since from the point of view of the mechanical behavior, significant differences were identified only between lipidic, calcified, and a generic plaque [20] (i.e., without a specific predominance of plaque components), in this work, it was decided to consider only CA and LT position data for modeling mechanical behaviors other than the generic plaque. Before coupling this information with the meshed artery, spatial filtering was applied to eliminate isolated points and other artifacts that would lead to an unrealistic representation of these tissues. Then, a Matlab script was employed to identify in which elements of the diseased intima each point was located. The strategy adopted for plaque modeling was based on the prevalence of identified plaque points within the element. Each element was considered as calcified plaque, lipid plaque, or generic plaque according to the following rule: the mesh element was described as a generic plaque if it had less than two points inside or, in case of two or more points inside, if there was not a prevalence of at least 70% of the points belonging to one of the two types. Otherwise, the mesh element was considered to belong to the plaque type to which at least 70% of the points inside the element belonged.

2.1.3. Mechanical Description of the Different Considered Tissues

For the mechanical description of coronary artery layers, the literature proposes complex constitutive models based on fiber reinforcement and able to replicate the anisotropic behavior of real tissues [19]. However, when modeling patient-specific reconstructed arteries, this approach is rarely applied and simpler models are generally preferred. In agreement with other literature works [16,21,22], for this application, the artery was described with an isotropic material model based on the circumferential behavior of real tissues.

To describe the media and adventitia layers, the following 6th order reduced polynomial strain energy density function (Equation (3)) was adopted:

$$U = C_{10}(\bar{I}_1 - 3) + C_{20}(\bar{I}_1 - 3)^2 + C_{30}(\bar{I}_1 - 3)^3 + C_{40}(\bar{I}_1 - 3)^4 + C_{50}(\bar{I}_1 - 3)^5 + C_{60}(\bar{I}_1 - 3)^6 \quad (3)$$

where U is the strain energy per unit of the reference volume, $\bar{I}_1$ is the first deviatoric strain invariant, and C_{i0} are the material parameters.

When patient-specific vessel anatomies are reconstructed based on in vivo clinical images, the stretched and pressurized vessel configurations are involved, whereas the experimental tests performed to obtain material data and derive constitutive model parameters are usually carried out on unloaded specimens of the tissue layers. To comprehensively model the mechanical behavior of the artery, it would be necessary to identify by inverse analysis the unloaded geometry of each coronary artery reconstructed from in

vivo images [23]. As an alternative to a time-consuming inverse analysis, however, to obtain a correct description of the mechanical response of in vivo coronary arteries, a suitable strategy was developed and explained as follows (Figure 2). An idealized coronary artery was modeled as a hollow cylinder with a lumen diameter equal to 2.7 mm, and the artery wall was divided into adventitia and media with 0.34 mm and 0.32 mm of thickness, respectively, according to the proportions reported in the literature [19]. The intima layer was not considered in the model since, generally, a healthy intima layer is 1 μm thick, and hence, its contribution to the load-carrying capability was assumed as negligible [24,25]. The fiber-reinforced models of Cilla et al. (2012) [14], calibrated on the experimental data obtained by Holzapfel et al. (2005) [19] in the circumferential and longitudinal directions of unloaded specimens of adventitia and media, were used in this study on the idealized artery as reference for the description of the mechanical behavior of both layers. An axial stretch equal to 4.4% of the vessel length and internal pressurization of 100 mmHg were applied to the idealized artery to mimic the in vivo status [19]. Then, the internal pressure was increased up to 600 mmHg to gain the stress-strain relation of the artery tissues beyond the physiological range (Figure 3). For both the adventitia and the media, the circumferential stress-strain relation highlighted by the simulation was used for deriving the constitutive parameters of Equation (3) (i.e., the equivalent isotropic model) considering the configuration after axial stretching and physiological pressurization as the unstressed condition. The fitting of the circumferential stress-strain relations of the two tissues led to the identification of the parameters of Equation (3) reported in Table 1. In this way, the equivalent isotropic model results to be already representative of an in vivo mechanical behavior allowing the description of the patient-specific arteries reconstructed based on in vivo clinical images. To verify the strategy and, in addition, the choice of calibrating the two isotropic material models on only the circumferential behavior of the arterial tissues, pressurization simulations of idealized diseased arteries were performed. Specifically, for the validation of this methodology, it was chosen to extend the comparison between isotropic and fiber-reinforced modeling to different sizes of the idealized artery considering a variation of ±0.5 mm to the 2.7 mm healthy lumen diameter (before pre-stretching and pressurization) used for the calibration of the material model parameters.

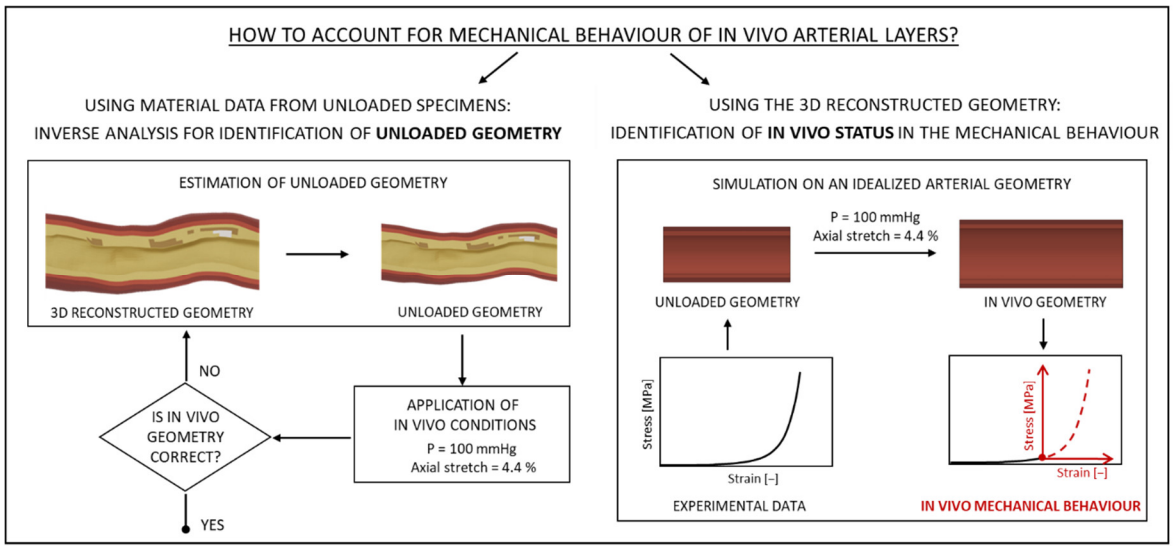

Figure 2. Schematic representation of two potential methods to account for the mechanical behavior of in vivo arterial layers as the experimental data to be associated with the reconstructed in vivo geometry are derived from testing unloaded specimens. On the left is shown a simplified scheme describing the rationale for identifying the unloaded geometry to be used with the experimental material data: by inverse analysis, the unloaded geometry is iteratively estimated from the geometry reconstructed from the in vivo images. On the right, an alternative, simpler method is proposed:

through simulations on an idealized arterial geometry of the artery, the working point corresponding to the in vivo status was identified in the experimental material data for the extrapolation of the in vivo mechanical behavior.

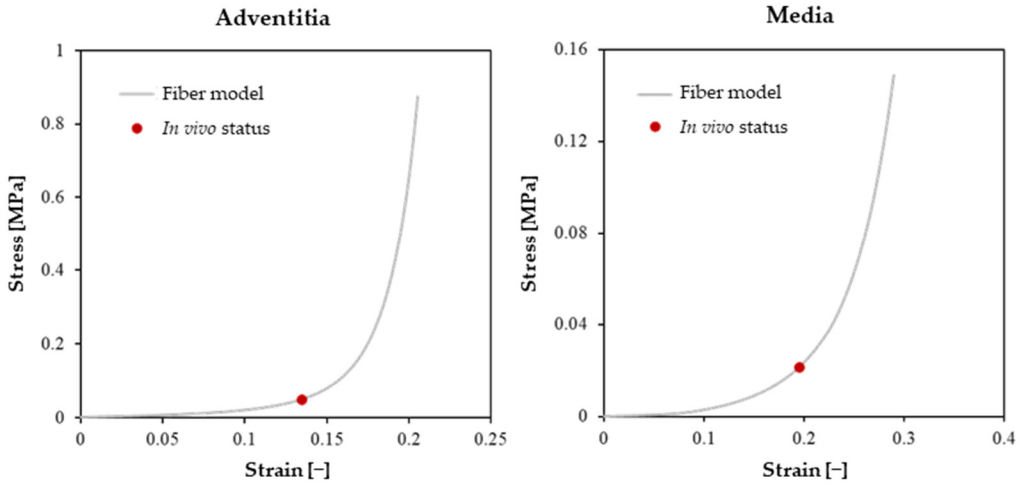

Figure 3. Circumferential stress-strain curves for adventitia (**left**) and media (**right**) described with the fiber-reinforced models obtained through the pre-stretching and pressurization of the two-layered cylinder. The red dots indicate the in vivo status configuration.

Table 1. Material models of adventitia and media: summary of the parameters of the 6th order reduced polynomial strain energy density function (Equation (3)) calibrated to fit the circumferential stress-strain curves of the fiber-reinforced model considering the in vivo status configuration as zero-condition.

	C_{10}	C_{20}	C_{30}	C_{40}	C_{50}	C_{60}
Adventitia	2.60×10^{-1}	4.76×10^{1}	-4.09×10^{3}	5.29×10^{5}	-2.69×10^{7}	5.65×10^{8}
Media	7.29×10^{-2}	3.71×10^{0}	-1.56×10^{2}	9.18×10^{3}	-2.61×10^{5}	2.91×10^{6}

In addition, a pathological state of the vessel was considered for each of these three vessel-size configurations, with the inclusion of a generic plaque layer (modeled as described below) such as to give a stenosis of 50% relative to the healthy lumen (Figure 4). The results of the pressurization simulations in terms of inner diameter were compared with those obtained with the fiber-reinforced models, as shown in Figure 4: the percentage error was always below 2%.

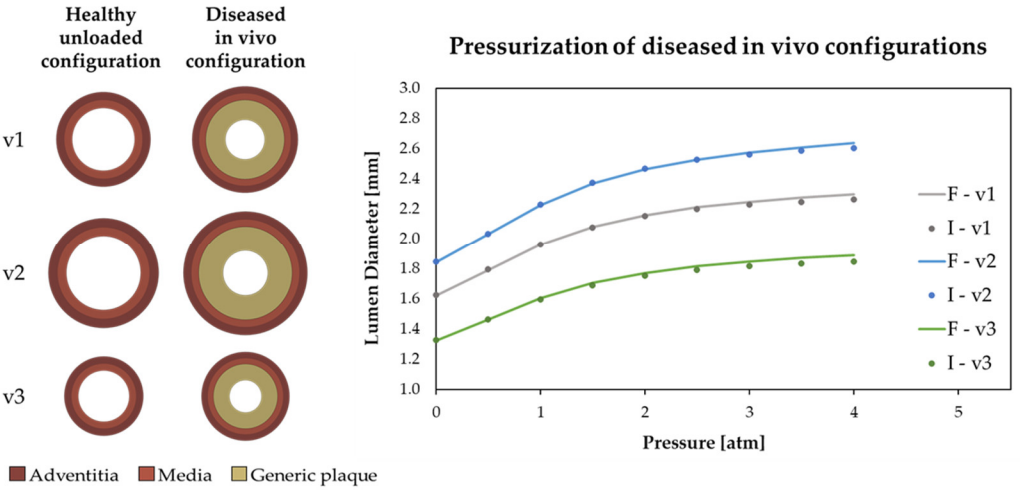

Figure 4. Validation of the strategy for modeling the media and adventitia layers with isotropic material calibrated on the circumferential in vivo behavior. On the left are the three different sizes of the healthy unloaded configuration of the idealized artery considered in the study: lumen diameters of the healthy unloaded artery of 2.7 mm (v1) (the one used for material calibration without the plaque), 3.2 mm (v2) and 2.2 mm (v3) were chosen. Starting from these geometries, three different configurations of diseased in vivo vessels were derived considering the deformations of media and adventitia under in vivo conditions and the addition of a generic plaque such as to model a 50% stenosis of the healthy lumen. Simulations of lumen pressurization of the three diseased in vivo configurations were performed for a comparison between the isotropic model calibrated on the in vivo circumferential behavior (I) and the fiber-reinforced model accounting for stresses and strains starting from the unloaded configuration (F). On the right are the simulation results in terms of lumen diameter versus the applied pressure increment beyond the physiological pressure value of 100 mmHg.

Once calibrated the elastic properties of the adventitia and the media (i.e., the hyperelastic model described by Equation (3), the softening of the mechanical response of the two artery tissues due to damage when subjected to high strains was phenomenologically represented by introducing a plastic behavior into the material model [3,21]. Specifically, a bilinear plastic hardening was adopted, in which upon reaching a certain strain value, the initial plastic stiffness is halved. The plastic parameters of the adventitia and the media are listed in Table 2.

Table 2. Plastic parameters for the adventitia and the media. The stress value corresponding to null plastic strain indicates the yielding stress.

Artery Tissue	Plastic Strain (–)	Plastic Stress (MPa)
Adventitia	0	1.60
	0.07	2.30
	0.40	4.00
Media	0	0.70
	0.07	1.10
	0.40	2.00

Concerning the plaque, the literature states that the mechanical properties of atherosclerotic coronary tissues are similar to those of the carotid [20]. A great variability in the stiffness values was observed: from 30–40 kPa [26] to 2 MPa [27], from 4 MPa [28] to 50 MPa [20], and from 10–20 kPa [26] to 0.5–1 MPa [29], respectively for generic plaque, calcified plaques and lipid plaques. Among these data, average stiffness values were chosen to describe the elastic behavior of the three plaque types. Neo-Hookean hyperelastic models were adopted for the generic and the lipid plaques, while the stiffer behavior of the calcified plaque was described with a linear elastic model. Both the generic plaque and the lipid plaque were assumed to be incompressible, hence the form of the neo-Hookean strain energy potential becomes:

$$U = C_{10}(\bar{I}_1 - 3) \quad (4)$$

where C_{10} is a material parameter, while U and $\bar{I}_1$ are the strain energy per unit of reference volume and the first deviatoric strain invariant, respectively. Differently, a compressible behavior with Poisson's ratio equal to 0.3 was chosen for the calcified plaques. Adopting the same strategy used for the mechanical description of the adventitia and the media, the potential damage of the different plaque components was represented with plastic models. In this case, ideal plasticity was selected: once the plastic field is reached, the stress remains constant at the yielding value despite the increase in plastic strain. The yielding values were selected based on the experimental data reported in Loree et al. (1994) [27]. Table 3 summarizes the material parameters of the three plaques.

Table 3. Summary of the material models and parameter values adopted for the mechanical description of the generic plaque, the lipid plaque, and the calcified plaque. For each plaque type, an ideal plastic behavior was adopted.

Plaque Type	Material Model	Material Parameters	Compressibility
Generic Plaque	Neo-Hookean Hyperelastic-Plastic	$C_{10} = 150$ KPa $\sigma_{yield} = 400$ KPa	Incompressible
Lipid Plaque	Neo-Hookean Hyperelastic-Plastic	$C_{10} = 13.3$ KPa $\sigma_{yield} = 70$ KPa	Incompressible
Calcified Plaque	Linear Elastic-Plastic	$E = 44$ MPa $\sigma_{yield} = 480$ KPa	Compressible, $\upsilon = 0.3$

2.2. In Silico Replication of the Treatment of the Two Patient-Specific Cases

Two patient-specific cases were selected within prospective clinical studies conducted by the University of Ioannina. The clinical study protocol conformed to the Declaration of Helsinki and was approved by the institutional ethics committee. All patients gave written informed consent. The selection of the clinical cases for this scientific work was based on specific requirements to limit the uncertainties of the model inputs. Specifically, concerning the artery, both pre-treatment clinical images for geometry reconstruction and post-treatment clinical images for comparison with FEA outcomes were required, with good image quality. In addition, it was essential to have detailed information about the clinical procedure to be able to faithfully replicate the treatment in silico. To further limit the uncertainties on the inputs, on the side of the devices used in the treatment, only clinical cases involving the SYNERGY™ Bioabsorbable Polymer Everolimus-Eluting Platinum Chromium Coronary Stent (Boston Scientific, Marlborough, MA, USA) were chosen, whose virtual model (Figure 5) was already validated in recent studies of the authors [10,30]. The two selected clinical cases, henceforth identified as Case A and Case B, which complied with the above requirements, were representative of two different levels of complexity in terms of the treatment site and the performed clinical procedure. Case A was characterized by a relatively short lesion section far from coronary bifurcations, while Case B was affected by a longer lesion involving a coronary bifurcation whose treatment required the implantation of two partially overlapped stents. However, since in Case B the clinical procedure did not include the treatment of the bifurcation side branch, it was not needed to reconstruct the side branch, but only the ostium presence was accounted for (Figure 6b). Regarding the clinical procedure, Case A required only two steps: a predilation of the stenotic lumen through balloon angioplasty followed by the stent implantation. The NC Solarice™ (Medtronic, Dublin, Ireland) balloon 2.50 mm × 15 mm (i.e., nominal diameter 2.50 mm and length 15 mm) was inflated up to 12 atm during angioplasty, while the stenting step involved the implantation of a SYNERGY™ stent 3.00 mm × 16 mm, at 14 atm. Case B, on the other hand, required a more complex procedure: the treatment included an angioplasty step with the inflation of NC Solarice™ balloon 2.50 mm × 27 mm at 14 atm, a first stenting step with distal SYNERGY™ stent 2.75 mm × 20 mm implantation at 12 atm, a second stenting step with proximal SYNERGY™ stent 3.00 mm × 28 mm implantation at 14 atm partially overlapping the previous stent and finally a post-dilation of the proximal stent with an NC Solarice™ balloon 3.50 mm × 20 mm at 16 atm. The comparison between Case A and Case B is summarized in Table 4.

Table 4. Clinical details of the two cases selected for this work.

Clinical Case	Lesion Length	% Diameter Stenosis	Procedure Step 1	Procedure Step 2	Procedure Step 3	Procedure Step 4
Case A	16 mm	60%	Angioplasty	Stenting	-	-
Case B	46 mm	69%	Angioplasty	Stenting 1	Stenting 2	Post-dilation

To have an accurate in silico replication of the two patient-specific cases, it was needed to have reliable models of the devices employed in the treatment. The collaboration with Boston Scientific Limited (BSL) within the InSilc project allowed the development of SYNERGY™ stent models starting from the knowledge of the correct material properties and geometries of the different device sizes. Some samples of the complete delivery system (provided by BSL) were used for in vitro testing to validate the stent and balloon models. Specifically, the virtual model was validated against free expansions, uniaxial tensile tests, and confined expansion tests. The description of the numerical model development and validation is reported in a recent study of the authors [10]. For NC Solarice™ balloon modeling, as done for the SYNERGY™ balloon, a multi-wings geometry and hyperelastic material behavior were chosen to ensure the achievement of the correct expanded diameters with respect to the inflation pressure [10,31,32]. Based on the knowledge of the balloon compliance charts, a specific model was made for each balloon involved in this study. Components such as the catheter and the guidewire play a marginal role in achieving the final configuration of the treated artery and, therefore, it was decided to neglect their modeling and to replicate only their effects within the simulation of the treatment. Numerical simulation of stent crimping was required before in silico replication of the artery treatment procedure. The action of the crimping machine was reproduced by a radial displacement of 16 rigid planes placed circumferentially around the stent and balloon [10,31,33]. The radial displacement of the planes was set to give a crimped stent representative of the real device in terms of outer diameter after the elastic recoil [10].

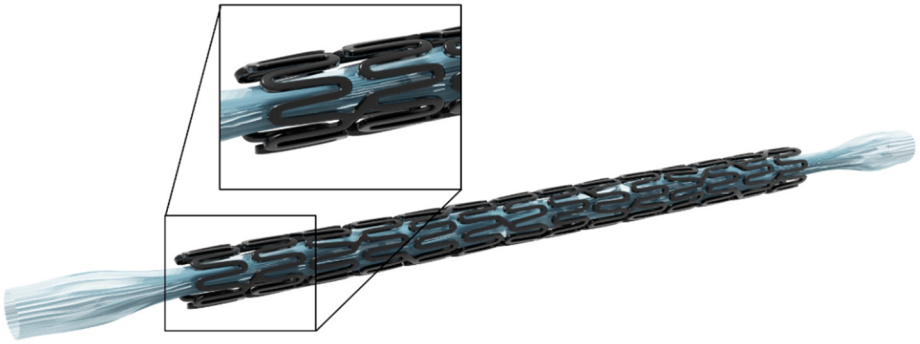

Figure 5. Virtual model of SYNERGY™ delivery system: stent and multi-wings balloon models after crimping simulation.

Each of the different procedures involved in the treatment of the two patient-specific cases consists of a sequence of three main steps: (i) positioning of the device (stent crimped on balloon or balloon alone for angioplasty or post-dilation) at the target site; (ii) balloon inflation, and (iii) balloon deflation. The reliability of the numerical method for in silico replication of these steps was evaluated in a previous study by comparison with in vitro deployment tests in deformable mock vessels [30]. For the device positioning, it was decided not to accurately reproduce the insertion of the catheter inside the artery, but to adapt the device to the vessel curvature directly at the target site. Specifically, the device deformation was driven by an external cylinder, at which nodes displacement conditions were applied to align the cylinder axis with the vessel centerline. As the information on the artery stented region was only available from post-treatment OCT images, to identify the position of the stent in the pre-treatment geometry, an association between the pre- and post-treatment images was required through the identification of landmarks. Moreover, the balloon position with respect to the artery or stent was replicated as faithfully as possible based on the information provided by the clinician. The balloon inflation step was performed by applying to the inner surface of the balloon a progressive increase of pressure up to the maximum value reached during the patient-specific clinical procedure.

Displacement constraints were imposed on the balloon extremities to replicate the attachment of the balloon to the catheter. Similarly, for the balloon deflation step, a progressive decrease in the inner pressure was applied to the balloon. Throughout the whole treatment simulation, the terminal sections of the artery model were kept fixed. However, to limit potential boundary effects, a vessel portion longer than the area to be treated was considered in the artery model. All the numerical simulations were performed using the commercial code Abaqus 2019 (Dassault Systemes, SIMULIA Corp., Johnston, RI, USA). Consistently with other literature works [3,7,30], due to the high nonlinearities involved in the simulations, the explicit solver was exploited, ensuring the quasi-static regime.

The comparison between the FEA prediction and the clinical outcomes recorded for the two patients was focused on the analysis of clinically relevant quantities such as lumen reopening and the correct apposition of the stent to the vessel wall. For the lumen reopening, it was decided to make a comparison in terms of the lumen area values along the entire stented section of the artery. For the clinical comparator, data on lumen areas were extracted from OCT images recorded pre- and post-treatment. Accounting for the distance between OCT slices, derived from the catheter pullback rate, the lumen area trend as a function of the vessel's axial coordinate was reconstructed. Similarly, for the simulation results, it was decided to section the 3D geometry with multiple cuts orthogonal to the vessel centerline to get the lumen area trend to be compared with the clinical data. Concerning the apposition of the stent to the vessel wall, both OCT and FEA slices were analyzed to identify potential regions where stent struts were not well apposed to the wall.

3. Results

Starting from the clinical images of the two patients, the sections of interest of each coronary artery were 3D reconstructed and meshed according to the rules defined in Section 2.1. The identification of plaque components suggested in the stented region a relevant presence of lipid plaque for case A with a volume percentage of 36% with respect to total plaque volume, compared with 14% of case B. For both cases, the calcified plaque was identified in localized spots with a volume percentage of less than 2%. The reconstructed geometry with the spatial distribution of the modeled artery components is shown in Figure 6 for both cases.

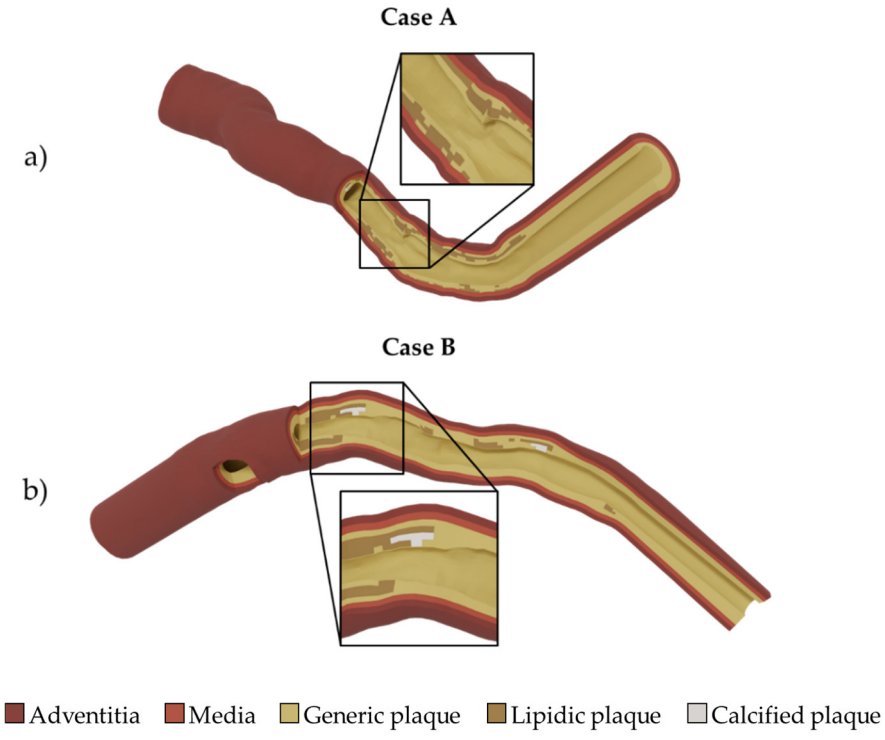

Figure 6. Sections of the 3D reconstructed geometries of the two patient-specific coronary arteries: (**a**) Case A and (**b**) Case B. The modeled components (adventitia, media, generic plaque, lipid plaque, and calcific plaque) were highlighted with different colors. For Case B bifurcation, the presence of the ostium was modeled without reconstruction of the untreated side branch.

The coronary artery models were evaluated, replicating the clinical treatments of Case A and Case B. The FEA results related to Case A are shown in Figure 7. As can be seen from the 3D artery section at the end of treatment, in the numerical simulation, the stent deployment was able to reduce the stenosis. The slices of the stented artery region, made by cuts orthogonal to the vessel centerline (Figure 7b), allowed the quantification of the lumen area for comparison with the clinical data. Figure 7c shows the values of lumen area as a function of the location along the vessel centerline. The post-treatment area derived from OCT images appears to be adequately estimated by FEA: a good fit between the graph curves can be seen along the whole stented region. Similarly, for Case B, starting from the 3D artery geometry at the end of treatment (Figure 8b), the area values estimated with FEA were compared with the clinical data. Figure 8a shows the good predictive capability of the model in assessing the area values achieved in post-treatment configuration, despite some local inaccuracies. As Case B involved a bifurcation in the stented region, the area affected by the bifurcation was not considered in the lumen area comparison. In both cases, a good apposition of the stent to the vessel wall along the entire stented region was predicted by the simulation, consistent with what was observed in post-treatment OCTs.

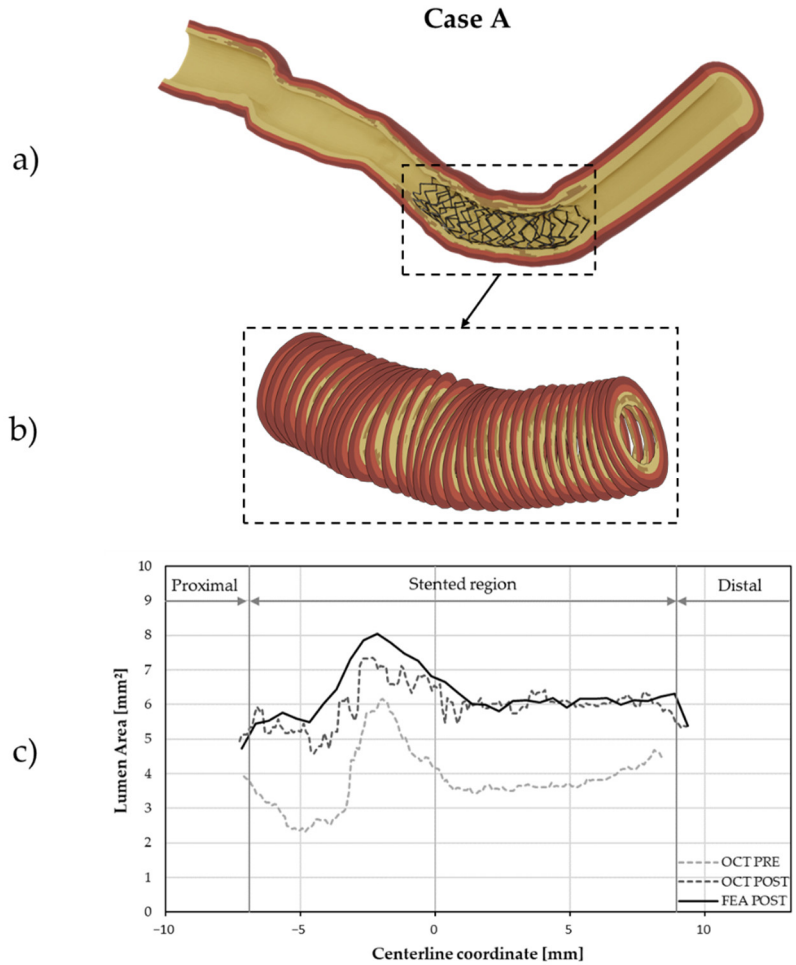

Figure 7. Numerical simulation results for the replication of Case A: (**a**) the geometry of artery section and stent at the end of clinical treatment; (**b**) slices orthogonal to the lumen centerline of the

stented artery region used for lumen area measurements; and (**c**) graph of the lumen area as a function of the centerline coordinate with the curves related to the clinical data deduced from pre- and post-treatment OCTs and the FEA results.

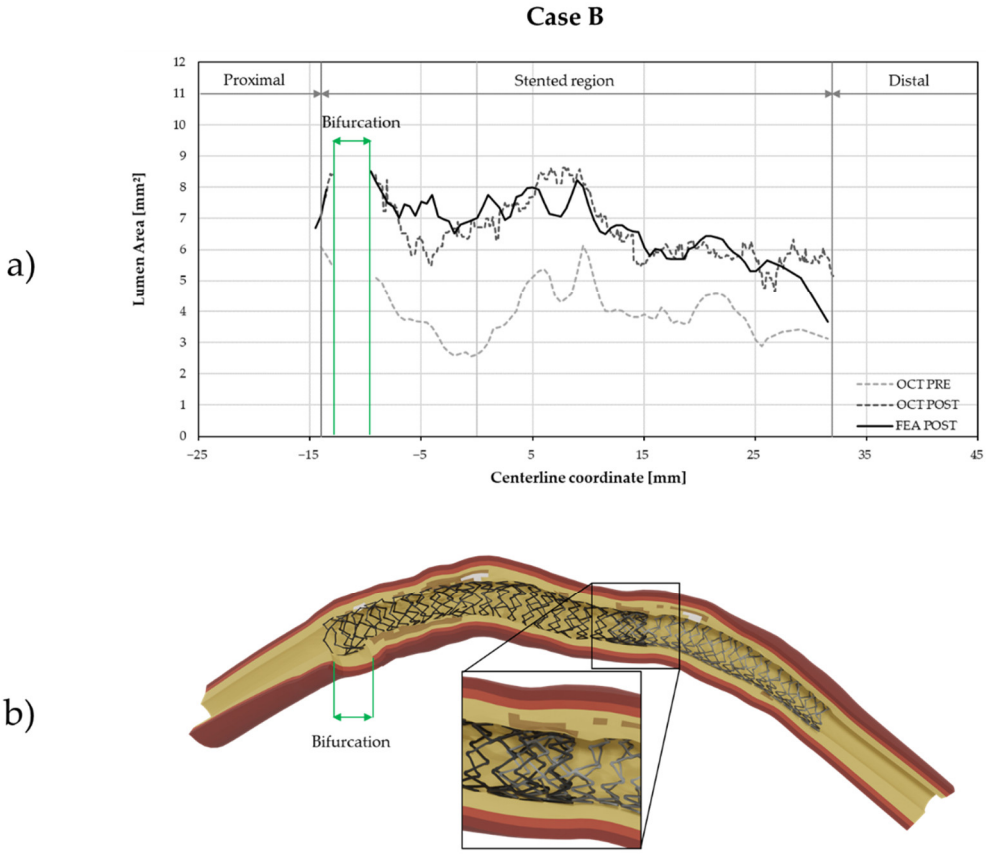

Figure 8. Numerical simulation results for the replication of Case B: (**a**) graph of the lumen area as a function of the centerline coordinate with the curves related to the clinical data deduced from pre- and post-treatment OCTs and the FEA results. The region corresponding to the bifurcation was not considered in the lumen area comparison; (**b**) the geometry of artery section and stent at the end of clinical treatment with detail on the region with overlapping stents.

4. Discussion

Concerning the artery reconstruction involved in the virtual representation of coronary stenting, since an image-based method was employed from start to finish, the quality of the resulting 3D models depended largely on the quality of the used images (Figure 1a). The 3D reconstruction and plaque characterization tool allows the automatic extraction of lumen and media outer border. One main problem in order to develop a 3D model using an OCT image was the extraction of the outer border of the adventitia layer. Due to the limited penetration depth of light, which is a characteristic of OCT, the adventitia outer border could not be consistently visible except in healthy or minimally diseased segments. Therefore, assumptions from the literature regarding the thickness of the layers were required. Another issue in implementing this image-based method was the noise of the image. Indeed, in many cases, blood artifacts existed inside the lumen, creating shadows and hiding the tissue morphology. The use of first- and second-generation wavelet filtering instead of bilateral filtering might be an improvement in reducing noise in the image [34,35].

The identification in a stress-strain diagram of the in vivo working point of the media and adventitia layers (Figure 3) turned out to be a fundamental aspect in modeling the mechanical behavior of the layers. Indeed, if the choice was made to assign mechanical

properties derived from tests on unloaded specimens directly to the in vivo reconstructed geometry of the artery as usually done in the literature, an underestimation of the layer stiffness would have resulted. In view of having a reliable but quick modeling of the patient-specific artery, the method developed to account for the artery in vivo status proved to be a good choice when compared with the need for an iterative process of inverse analysis to identify the unloaded geometry. Indeed, looking at outcomes of clinical interest such as the lumen opening under pressure loading, the comparison shown in Figure 4 between an isotropic model with as zero-configuration the in vivo status and a fiber-reinforced model accounting for the real stress state shows a good match of results. This showed how it is possible to develop a suitable phenomenological approach that replicates the performance in terms of circumferential mechanical response.

The identification in a stress–strain diagram of the in vivo working point of the media and adventitia layers (Figure 3), turned out to be a fundamental aspect in modeling the mechanical behavior of the layers. Indeed, if the choice was made to assign mechanical properties derived from tests on unloaded specimen directly to the in vivo reconstructed geometry of the artery as usually done in the literature, an underestimation of the layer stiffness would have resulted. In view of having a reliable but quick modeling of the patient-specific artery, the method developed to account for the artery in vivo status proved to be a good choice when compared with the need for an iterative process of inverse analysis to identify the unloaded geometry. Indeed, looking at outcomes of clinical interest such as lumen opening under pressure loading, the comparison shown in Figure 4 between an isotropic model with as zero-configuration the in vivo status and a fiber-reinforced model accounting for the real stress state shows a good match of results. This showed how it is possible to develop a suitable phenomenological approach that replicates the performance in terms of circumferential mechanical response.

The effectiveness of this modeling approach, coupled with the identification of mesh elements to be described as generic plaque, calcific plaque, or lipid plaque depending on what was observed from clinical images, was assessed by simulating the treatment procedure of two patient-specific arteries. The choice of cases on which to perform these assessments fell on two patients treated with clinical procedures of different complexity level: from a simple angioplasty followed by stent implantation (Case A) to an angioplasty followed by the deployment of two partially overlapped stent and completed by a final post-dilation (Case B). In addition, thanks to previous works by the authors [10,30] validating the models of the stents involved in both treatments and the numerical strategy for deployment simulation, it was possible to limit the uncertainties associated with the virtual representation of the two cases for a more accurate assessment of the patient-specific artery modeling.

The comparison of the results obtained by simulating stent implantation with what was observed on post-treatment clinical images demonstrated the efficiency of the developed artery models. When performing this assessment, it is necessary to take into account the uncertainties that affect both the simulation and the comparator. Indeed, the reconstruction process is potentially conditioned by the presence of artifacts that could lead to the generation of a reconstructed geometry very similar but not perfectly superimposable to the real artery. Therefore, given the uncertainties that affect both numerical results (uncertainties in vessel reconstruction) and in vivo data (uncertainties in segmentation of the post-treatment images), the results are to be considered in good overlap in both clinical cases. A phenomenological description of the artery is therefore reasonable when the goal is to analyze quantities such as lumen reopening after stent implantation.

A further aspect that the model allows to evaluate is the apposition of the stent to the vessel wall, which information can be hardly accessible in common clinical practice. In both the patient-specific cases, the virtual model predicted complete stent apposition to the vessel wall in accordance with post-treatment OCTs. Although no stent malapposition was directly encountered in these clinical cases, it is expected that the model would be

able to predict malapposition risks when present. Moreover, it is believed that the numerical simulation could represent a tool for the identification of tissue regions with high stretch and a possible risk of arterial injuries, providing a virtual insight on the treatment outcome.

It is worth noting that for both the patient-specific cases, the same mean literature values were used for the material model parameters of the arterial and plaque components. Nevertheless, an accurate patient-specific spatial distribution of the plaque components was accounted for, as well individual values for media and adventitia thicknesses were adopted. The satisfactory simulation results indicate that the plaque features and the wall thickness are the main determinants of arterial stiffness. However, this conclusion should be verified on a larger number of patients, as the need for fine-tuning of material parameters in other patient-specific cases cannot be excluded.

The employment of virtual representations of patient-specific treatments like coronary stenting to be able to provide virtual insights on the treatment outcome recalls the industrial concept of the digital twin. In its classical meaning, a digital twin is a virtual model fed by sensors placed on the physical system, which allow its real-time monitoring; in turn, the digital twin produces virtual insights and data, which would be impossible to obtain through direct observation of the real object. In the biomedical context, we can figure out two different concepts for defining a digital twin. The first one, very similar to the original definition, can be applied to implantable active devices such as insulin pumps or pacemakers. These are components where the implant phase is not critical, while it could be important to adapt their functioning according to the patient response. Hence, they could be potentially monitored by continuous data acquisition, allowing real-time interaction with a digital twin (of both the device and the physiological system of interest) and better control. Regarding the second application of digital twin in a biomedical context, when a clinical treatment involving the interaction of a device with the biological structure is computationally modeled (e.g., a stenting procedure), the classical definition needs to be partially reformulated. Indeed, when a continuous acquisition by sensors is impossible, the interaction between reality and virtual model can only occur at discrete and limited times. Furthermore, the data required as input by the model usually involve a 3D description of the biological counterpart rather than simple clinical measures. This is the case of interventional cardiology (but also for orthopedic prosthesis implantation), where patient's data for a potential digital twin can be acquired only through clinical images collected before, during, and after treatment. In this context, the digital twin should be considered as an in silico tool that integrates clinical data acquired at suitable times and uses simulation results to support clinical decisions.

As already mentioned, some computational models based on patient images currently exist with specific reference to coronary diseases [13], which are exploited for performing hemodynamic simulations and guiding the disease diagnosis. In these cases, the images (coronary computed tomography angiography, CCTA) are acquired non-invasively and the times needed for model implementation and simulation execution (hours) are compatible with the clinical activity: hence, the computational model can be considered as a digital twin, which is informed by clinical images and measurements (the sensors), and is able to interact with the real system (the clinics) by indicating to the clinicians whether a coronary stenosis has to be treated or not.

Although the clinical conditions are quite different, a digital twin can also be the virtual representation of a coronary stent deployment as that described in this study, which however requires methods for the patient-specific artery reconstruction, nowadays based on catheter-based imaging techniques such as optical coherence tomography (OCT) or intravascular ultrasound. Considering that these clinical images, due to their invasiveness, can be acquired only during the surgical procedure in which the stent is implanted, it is obvious that the current computational times (some hours for FEA) are not compatible with the clinical needs and that the use of a digital twin for supporting the treatment (i.e., the stenting procedure) is currently unfeasible.

However, a digital twin of coronary stenting based on images collected during the procedure could be used today for better planning of the patient follow-up, providing the clinicians with useful information, predictors of the subsequent biological response, not directly obtainable from the post-treatment images. Finally, by complementing the stent deployment model simulations with additional hemodynamics, drug release, and stent degradation (for bioresorbable stents) simulations, a more complete and useful digital twin of the treatment outcome can be developed.

5. Conclusions

The good overlap of results obtained from stent deployment simulations compared to in vivo data demonstrated the effectiveness of the artery modeling method proposed in this work, as well as the accuracy in mimicking the stenting procedure. In both the investigated stenting cases, only in some spots there are discrepancies between in vivo and in silico lumen area measurements, but considering the uncertainties related to the analysis of clinical images that inevitably affect both the 3D reconstruction of the pre-treatment artery and the profile of the post-treatment lumen area, the results must be considered satisfactory. The isotropic material model calibrated on the circumferential mechanical behavior of the media and adventitia tissues conveniently allowed to account for the artery in vivo conditions and have good performance when aiming at quantities such as lumen reopening following stent deployment. It also allows containing the computational time, which nevertheless remains incompatible with a real-time assessment of treatment outcome. However, it is believed that the virtual model of the patient-specific stenting treatment could provide virtual insights about other interesting quantities associated with the clinical treatment (e.g., wall stresses) towards specific planning of the patient follow-up. In addition, with the potential exploitation of new non-invasive imaging techniques for the reconstruction of the patient artery before the surgical act, future application of the coronary stenting digital twin for treatment planning is not excluded.

Author Contributions: Conceptualization, L.P. and G.P. (Giancarlo Pennati); methodology, G.P. (Giancarlo Pennati); software, G.P. (Gianluca Poletti), L.A., L.M. and P.T.; validation, G.P. (Gianluca Poletti), L.A. and L.M.; formal analysis, G.P. (Gianluca Poletti) and L.A.; investigation, G.P. (Gianluca Poletti), L.A., L.M., P.T., M.I.P. and L.K.M.; resources, G.S.K., D.I.F., L.P. and G.P. (Giancarlo Pennati); data curation, G.P. (Gianluca Poletti), L.A., M.I.P. and L.K.M.; writing—original draft preparation, G.P. (Gianluca Poletti), L.A. and G.S.K.; writing—review and editing, G.P. (Gianluca Poletti), L.A., L.P. and G.P. (Giancarlo Pennati); visualization, G.P. (Gianluca Poletti); supervision, L.P. and G.P. (Giancarlo Pennati); project administration, G.P. (Giancarlo Pennati); funding acquisition, G.S.K., D.I.F., L.P. and G.P. (Giancarlo Pennati). All authors have read and agreed to the published version of the manuscript.

Funding: This project received funding from the European Union's Horizon 2020 research and innovation program under grant agreement n° 777119. This article reflects only the authors' view and the Commission is not responsible for any use that may be made of the information it contains. This research was partially funded by MIUR FISR—FISR2019_03221 CECOMES.

Institutional Review Board Statement: The study was conducted in accordance with the Declaration of Helsinki, and approved by the Institutional Review Board (or Ethics Committee) of University of Ioannina (Approval no. 35-168, 26 November 2018).

Informed Consent Statement: Informed consent was obtained from all subjects involved in the study.

Data Availability Statement: Virtual population datasets is available in the following link https://www.cardiovascularvirtualpopulation.eu/ (accessed on 17 December 2021).

Acknowledgments: The authors would like to thank Boston Scientific Limited for their support and collaboration on this work.

Conflicts of Interest: The authors declare no conflict of interest. The funders had no role in the design of the study; in the collection, analyses, or interpretation of data; in the writing of the manuscript, or in the decision to publish the results.

References

1. Timmis, A.; Townsend, N.; Gale, C.P.; Torbica, A.; Lettino, M.; Petersen, S.E.; Mossialos, E.A.; Maggioni, A.P.; Kazakiewicz, D.; May, H.T.; et al. European society of cardiology: Cardiovascular disease statistics 2019. *Eur. Heart J.* **2020**, *41*, 12–85. https://doi.org/10.1093/eurheartj/ehz859.
2. Byrne, R.A.; Joner, M.; Kastrati, A. Stent thrombosis and restenosis: What have we learned and where are we going? the Andreas Grüntzig Lecture ESC 2014. *Eur. Heart J.* **2015**, *36*, 3320–3331. https://doi.org/10.1093/eurheartj/ehv511.
3. Chiastra, C.; Wu, W.; Dickerhoff, B.; Aleiou, A.; Dubini, G.; Otake, H.; Migliavacca, F.; LaDisa, J.F. Computational replication of the patient-specific stenting procedure for coronary artery bifurcations: From OCT and CT imaging to structural and hemodynamics analyses. *J. Biomech.* **2016**, *49*, 2102–2111. https://doi.org/10.1016/j.jbiomech.2015.11.024.
4. Conway, C.; McGarry, J.P.; Edelman, E.R.; McHugh, P.E. Numerical Simulation of Stent Angioplasty with Predilation: An Investigation into Lesion Constitutive Representation and Calcification Influence. *Ann. Biomed. Eng.* **2017**, *45*, 2244–2252. https://doi.org/10.1007/s10439-017-1851-3.
5. He, R.; Zhao, L.G.; Silberschmidt, V.V.; Liu, Y.; Vogt, F. Patient-specific modelling of stent overlap: Lumen gain, tissue damage and in-stent restenosis. *J. Mech. Behav. Biomed. Mater.* **2020**, *109*, 103836. https://doi.org/10.1016/j.jmbbm.2020.103836.
6. He, R.; Zhao, L.; Silberschmidt, V.V.; Liu, Y.; Vogt, F. Computational Evaluation of Artery Damage in Stent Deployment. *Procedia Struct. Integr.* **2018**, *13*, 187–191. https://doi.org/10.1016/j.prostr.2018.12.031.
7. Morlacchi, S.; Colleoni, S.G.; Cárdenes, R.; Chiastra, C.; Diez, J.L.; Larrabide, I.; Migliavacca, F. Patient-specific simulations of stenting procedures in coronary bifurcations: Two clinical cases. *Med. Eng. Phys.* **2013**, *35*, 1272–1281. https://doi.org/10.1016/j.medengphy.2013.01.007.
8. Samant, S.; Wu, W.; Zhao, S.; Khan, B.; Sharzehee, M.; Panagopoulos, A.; Makadia, J.; Mickley, T.; Bicek, A.; Boismier, D.; et al. Computational and experimental mechanical performance of a new everolimus-eluting stent purpose-built for left main interventions. *Sci. Rep.* **2021**, *11*, 8728. https://doi.org/10.1038/s41598-021-87908-2.
9. Migliavacca, F. Is modeling stents still an important issue? *Procedia Struct. Integr.* **2019**, *15*, 46–50. https://doi.org/10.1016/j.prostr.2019.07.009.
10. Antonini, L.; Mandelli, L.; Berti, F.; Pennati, G.; Petrini, L. Validation of the computational model of a coronary stent: A fundamental step towards in silico trials. *J. Mech. Behav. Biomed. Mater.* **2021**, *122*, 104644. https://doi.org/10.1016/j.jmbbm.2021.104644.
11. Tao, F.; Cheng, J.; Qi, Q.; Zhang, M.; Zhang, H.; Sui, F. Digital twin-driven product design, manufacturing and service with big data. *Int. J. Adv. Manuf. Technol.* **2018**, *94*, 3563–3576. https://doi.org/10.1007/s00170-017-0233-1.
12. Corral-Acero, J.; Margara, F.; Marciniak, M.; Rodero, C.; Loncaric, F.; Feng, Y.; Gilbert, A.; Fernandes, J.F.; Bukhari, H.A.; Wajdan, A.; et al. The "Digital Twin" to enable the vision of precision cardiology. *Eur. Heart J.* **2020**, *41*, 4556–4564.
13. Min, J.K.; Taylor, C.A.; Achenbach, S.; Koo, B.K.; Leipsic, J.; Nørgaard, B.L.; Pijls, N.J.; De Bruyne, B. Noninvasive fractional flow reserve derived from coronary CT angiography. *JACC Cardiovasc. Imaging* **2015**, *8*, 1209–1222. http://dx.doi.org/10.1016/j.jcmg.2015.08.006.
14. Cilla, M.; Peña, E.; Martínez, M.A. 3D computational parametric analysis of eccentric atheroma plaque: Influence of axial and circumferential residual stresses. *Biomech. Model. Mechanobiol.* **2012**, *11*, 1001–1013. https://doi.org/10.1007/s10237-011-0369-0.
15. Bukala, J.; Kwiatkowski, P.; Malachowski, J. Numerical analysis of stent expansion process in coronary artery stenosis with the use of non-compliant balloon. *Biocybern. Biomed. Eng.* **2016**, *36*, 145–156. https://doi.org/10.1016/j.bbe.2015.10.009.
16. Ragkousis, G.E.; Curzen, N.; Bressloff, N.W. Computational Modelling of Multi-folded Balloon Delivery Systems for Coronary Artery Stenting: Insights into Patient-Specific Stent Malapposition. *Ann. Biomed. Eng.* **2015**, *43*, 1786–1802. https://doi.org/10.1007/s10439-014-1237-8.
17. Frangi, A.F.; Niessen, W.J.; Vincken, K.L.; Viergever, M.A. Multiscale vessel enhancement filtering. In Proceedings of the Medical Image Computing and Computer-Assisted Intervention—MICCAI'98, Cambridge, MA, USA, 11–13 October 1998; Wells, W.M., Colchester, A., Delp, S., Eds.; Springer: Berlin/Heidelberg, Germany, 1998; pp. 130–137.
18. Tsompou, P.I.; Andrikos, I.O.; Karanasiou, G.S.; Sakellarios, A.I.; Tsigkas, N.; Kigka, V.I.; Kyriakidis, S.; Michalis, L.K.; Fotiadis, D.I.; Author, S.B. Validation study of a novel method for the 3D reconstruction of coronary bifurcations. *Proc. Annu. Int. Conf. IEEE Eng. Med. Biol. Soc. EMBS* **2020**, *2020*, 1576–1579. https://doi.org/10.1109/EMBC44109.2020.9176178.
19. Holzapfel, G.A.; Sommer, G.; Gasser, C.T.; Regitnig, P. Determination of layer-specific mechanical properties of human coronary arteries with nonatherosclerotic intimal thickening and related constitutive modeling. *Am. J. Physiol.-Hear. Circ. Physiol.* **2005**, *289*, 2048–2058. https://doi.org/10.1152/ajpheart.00934.2004.
20. Akyildiz, A.C.; Speelman, L.; Gijsen, F.J.H. Mechanical properties of human atherosclerotic intima tissue. *J. Biomech.* **2014**, *47*, 773–783. https://doi.org/10.1016/j.jbiomech.2014.01.019.
21. Gastaldi, D.; Morlacchi, S.; Nichetti, R.; Capelli, C.; Dubini, G.; Petrini, L.; Migliavacca, F. Modelling of the provisional side-branch stenting approach for the treatment of atherosclerotic coronary bifurcations: Effects of stent positioning. *Biomech. Model. Mechanobiol.* **2010**, *9*, 551–561. https://doi.org/10.1007/s10237-010-0196-8.
22. Pant, S.; Bressloff, N.W.; Limbert, G. Geometry parameterization and multidisciplinary constrained optimization of coronary stents. *Biomech. Model. Mechanobiol.* **2012**, *11*, 61–82. https://doi.org/10.1007/s10237-011-0293-3.
23. Chandra, S.; Gnanaruban, V.; Riveros, F.; Rodriguez, J.F.; Finol, E.A. A methodology for the derivation of unloaded abdominal aortic aneurysm geometry with experimental validation. *J. Biomech. Eng.* **2016**, *138*, 101005. https://doi.org/10.1115/1.4034425.

24. Favero, G.; Paganelli, C.; Buffoli, B.; Rodella, L.F.; Rezzani, R. Endothelium and its alterations in cardiovascular diseases: Life style intervention. *BioMed Res. Int.* **2014**, *2014*, 801896. https://doi.org/10.1155/2014/801896.
25. Gasser, T.C.; Ogden, R.W.; Holzapfel, G.A. Hyperelastic modelling of arterial layers with distributed collagen fibre orientations. *J. R. Soc. Interface* **2006**, *3*, 15–35. https://doi.org/10.1098/rsif.2005.0073.
26. Chai, C.K.; Akyildiz, A.C.; Speelman, L.; Gijsen, F.J.H.; Oomens, C.W.J.; van Sambeek, M.R.H.M.; van der Lugt, A.; Baaijens, F.P.T. Local axial compressive mechanical properties of human carotid atherosclerotic plaques-characterisation by indentation test and inverse finite element analysis. *J. Biomech.* **2013**, *46*, 1759–1766. https://doi.org/10.1016/j.jbiomech.2013.03.017.
27. Loree, H.M.; Grodzinsky, A.J.; Park, S.Y.; Gibson, L.J.; Lee, R.T. Static circumferential tangential modulus of human atherosclerotic tissue. *J. Biomech.* **1994**, *27*, 195–204. https://doi.org/10.1016/0021-9290(94)90209-7.
28. Maher, E.; Creane, A.; Sultan, S.; Hynes, N.; Lally, C.; Kelly, D.J. Tensile and compressive properties of fresh human carotid atherosclerotic plaques. *J. Biomech.* **2009**, *42*, 2760–2767. https://doi.org/10.1016/j.jbiomech.2009.07.032.
29. Lawlor, M.G.; O'Donnell, M.R.; O'Connell, B.M.; Walsh, M.T. Experimental determination of circumferential properties of fresh carotid artery plaques. *J. Biomech.* **2011**, *44*, 1709–1715. https://doi.org/10.1016/j.jbiomech.2011.03.033.
30. Berti, F.; Antonini, L.; Poletti, G.; Fiuza, C.; Vaughan, T.J.; Migliavacca, F.; Petrini, L.; Pennati, G. How to Validate in silico Deployment of Coronary Stents: Strategies and Limitations in the Choice of Comparator. *Front. Med. Technol.* **2021**, *3*, 702656. https://doi.org/10.3389/fmedt.2021.702656.
31. Antonini, L.; Berti, F.; Isella, B.; Hossain, D.; Mandelli, L.; Pennati, G.; Petrini, L. From the real device to the digital twin: A coupled experimental-numerical strategy to investigate a novel bioresorbable vascular scaffold. *PLoS ONE* **2021**, *16*, e0252788. https://doi.org/10.1371/journal.pone.0252788.
32. Chiastra, C.; Grundeken, M.J.; Collet, C.; Wu, W.; Wykrzykowska, J.J.; Pennati, G.; Dubini, G.; Migliavacca, F. Biomechanical Impact of Wrong Positioning of a Dedicated Stent for Coronary Bifurcations: A Virtual Bench Testing Study. *Cardiovasc. Eng. Technol.* **2018**, *9*, 415–426. https://doi.org/10.1007/s13239-018-0359-9.
33. Antonini, L.; Poletti, G.; Mandelli, L.; Dubini, G.; Pennati, G.; Petrini, L. Comprehensive computational analysis of the crimping procedure of PLLA BVS: Effects of material viscous-plastic and temperature dependent behavior. *J. Mech. Behav. Biomed. Mater.* **2021**, *123*, 104713. https://doi.org/10.1016/j.jmbbm.2021.104713.
34. Ahmed, S.S.; Messali, Z.; Ouahabi, A.; Trepout, S.; Messaoudi, C.; Marco, S. Nonparametric denoising methods based on contourlet transform with sharp frequency localization: Application to low exposure time electron microscopy images. *Entropy* **2015**, *17*, 3461–3478. https://doi.org/10.3390/e17053461.
35. Ouahabi, A. A review of wavelet denoising in medical imaging. In Proceedings of the 8th International Workshop on Systems, Signal Processing and Their Application (IEEE/WoSSPA), Algeris, Algeria, 12–15 May 2013; pp. 19–26.